Final version published as: Jannesar, S., Allen, M., Mills, S., Gibbons, A., Bresnahan, J. C., Salegio, E. A., & Sparrey, C. J. (2018). Compressive mechanical characterization of non-human primate spinal cord white matter. Acta Biomaterialia, 74, 260–269. https://doi.org/10.1016/j.actbio.2018.05.002.

Acta Biomaterialia

Title Page

Compressive mechanical characterization of non-human primate spinal cord white matter

Shervin Jannesar[1], Mark Allen[2], Sarah Mills[2], Anne Gibbons[2], Jacqueline C. Bresnahan[3], Ernesto A. Salegio[2] and Carolyn J. Sparrey[1,4]*

[1]Mechatronic Systems Engineering, Simon Fraser University, Surrey, BC Canada

[2]California National Primate Research Center, University of California Davis, CA, USA

[3]Department of Neurological Surgery, Brain and Spinal Injury Center, University of California at San Francisco, San Francisco, CA, USA

[4]International Collaboration on Repair Discoveries (ICORD), Vancouver, BC Canada

***Corresponding Author:**

Carolyn J. Sparrey, PhD

Associate Professor

Simon Fraser University

250-13450 102 Ave, Surrey, BC, V3T 0A3, CANADA

phone: (778) 782-8938

email: csparrey@sfu.ca

Running Title: Compressive mechanical characterization of non-human primate spinal cord white matter

Keywords: spinal cord injury; non-human primate; white matter; tissue characterization; viscoelastic constitutive model

ABSTRACT

The goal of developing computational models of spinal cord injury (SCI) is to better understand the human injury condition. However, finite element models of human SCI have used rodent spinal cord tissue properties due to a lack of experimental data. Central nervous system tissues in non human primates (NHP) closely resemble that of humans and therefore, it is expected that material constitutive models obtained from NHPs will increase the fidelity and the accuracy of human SCI models. Human SCI most often results from compressive loading and spinal cord white matter properties affect FE predicted patterns of injury; therefore, the objectives of this study were to characterize the unconfined compressive response of NHP spinal cord white matter and present an experimentally derived, finite element tractable constitutive model for the tissue. Cervical spinal cords were harvested from nine male adult NHPs (*Macaca mulatta*). White matter biopsy samples (3mm in diameter) were taken from both lateral columns of the spinal cord and were divided into four strain rate groups for unconfined dynamic compression and stress relaxation (post-mortem <1-hour). The NHP spinal cord white matter compressive response was sensitive to strain rate and showed substantial stress relaxation confirming the viscoelastic behavior of the material. An Ogden 1st order model best captured the non-linear behavior of NHP white matter in a quasi-linear viscoelastic material model with 4-term Prony series. This study is the first to characterize NHP spinal cord white matter at high (>10/sec) strain rates typical of traumatic injury. The finite element derived material constitutive model of this study will increase the fidelity of SCI computational models and provide important insights for transferring pre-clinical findings to clinical treatments.

1 INTRODUCTION

With recent progresses in spinal cord injury (SCI) pre-clinical trials [1,2], computational models of SCI have emerged as a powerful platform to bridge pre-clinical findings to humans as well as providing constructive insights into SCI mechanisms [3–5]. However, the fidelity and the accuracy of these computational models are critically dependent on their pre-defined material constitutive models [6,7]. By necessity, the majority of existing SCI computational models have used material constitutive models obtained from rodent [3–5,8,9] or porcine/bovine [10,11] tissue characterization. However, due to substantial morphological and physiological heterogeneity between these species and humans, examining a more human-like tissue and quantifying its constitutive properties is expected to improve the fidelity of human injury computational models.

SCI can occur from a range of loading mechanisms [12]. Contusion SCIs are the most common type of injury observed clinically and used experimentally [13,14]. Characterization of these injuries *in vivo*, *ex vivo* and mathematically have shown a multiaxial state of strain/stress at the tissue level as a result of the injury [1,3,8,15–17]. Moreover, differentiating individual tissue characteristics (e.g. grey and white matters and pia mater) is necessary to more accurately predict patterns of injury across the cord structure [10,18]. There is significant evidence that suggests the spinal cord white matter structure is transversely isotropic due to the rostral-caudal alignment of axonal fibers in the white matter [19,20]. Therefore, the direction of loading (e.g. mechanical testing) affects the observed material properties of the white matter.

Approaches to modelling transversely isotropic neurological materials include introducing the directional dependency of the material deformation into the strain energy function [21,22]. A first step in characterizing such materials is to characterize the material’s matrix [23,24]. The

longitudinally aligned axonal fibers in the white matter are embedded in a glial matrix that is devoid of a collagenous, structural extracellular matrix and has isotropic material properties [20]. Since the mechanical resistance of the fibers to compression in the fiber direction is negligible [25,26], rostro-caudal compressive testing of the white matter determines the isotropic isolated matrix characteristics with a negligible contribution of the fibers. Using more human-like subjects (NHPs) in this study will expand our understanding of the spinal cord white matter glial matrix and provide the opportunity to compare tissue characteristics between species. Further study is required to characterize the axonal fibers to augment the matrix characteristics to fully characterize the transversely isotropic material properties of spinal cord white matter [10,18,24,26]. However, this is a complex challenge due to the scale of available spinal cord white matter tissue samples (< 2 mm).

Unconfined compression tests have been used to characterize spinal cord [14,18] and brain [27–32] white matter from a range of species. Despite advances in characterizing the brain tissue, differences in the biological responses of brain and spinal cord [33,34] and their corresponding structural difference (e.g. fiber orientation, density and alignment) have restricted the use of brain white matter characteristics for the spinal cord. Spinal cord white matter has been characterized using quasi-static [5,18], 0.5 to 0.005 mm/sec deformation velocities [35] and 0.005/sec to 5.0/sec strain rate test data [14]. More recently, whole cords have been characterized using non-linear viscoelastic models for low strains (<5%) and moderate strain rates (0.1/sec) [36]. However, during a typical traumatic SCI the spinal cord undergoes large deformations at strain rates of approximately 110/sec [37,38]. Knowing that the impact velocity substantially affects the pattern and severity of the SCI [39], characterizing the tissue at higher strain rates is crucial for more accurate SCI models. Existing computational models of SCI have adopted viscoelastic parameters

from brain studies [3,8,40], however, applying a constitutive model obtained from combining spinal cord and brain tissues neglects the tissue specific characteristics. Furthermore, the degenerative effects of time post-mortem on the mechanical properties of the neurological tissues have been acknowledged [41,42]. Tissue degradation starts quickly after animal sacrifice due to complex enzymatic and microbiological processes [30,41,42]. However, due to difficulties in accessing the tissue and testing logistics, the time post-mortem has exceeded 3 hours in published spinal cord experiments [14,35,43,44]. The tangent modulus of the spinal cord tissue has been reported to nearly double over the period of 3 to 72 hours post-mortem [42]. To minimize the effect of post mortem degradation on the measured tissue characteristics samples should tested as soon as possible after death. This study aimed to characterize freshly harvested (post-mortem time < 1 hour) NHP spinal cord white matter at high strain rates using unconfined compression testing to better approximate the *in vivo* tissue response.

The goal of this study was to characterize the NHP spinal cord white matter mechanical behavior using fresh specimen and at high strain rates (as compared to existing studies). Specific objectives were to: (1) measure the time dependent mechanical response of the NHP spinal cord white matter through unconfined uniaxial compressive tests at strain rates approaching traumatic SCI rates; (2) explore the effects of applied strain rate on the NHP spinal cord white matter mechanical response; and (3) to determine a time-dependent material model with optimized material parameters capable of capturing the NHP spinal cord white matter mechanical behavior.

2 METHODS

2.1 Experiment

Spinal cords were collected for unconfined compression testing from the cervical spines (C1-C7) of nine adolescent (52.6±5.9 months old) male *Macaca mulatta* NHPs (7.44±1.31kg) immediately (<20minutes) after euthanasia. The spinal cords were detached from the spinal canal by cutting through denticulate ligaments and the nerve roots. Dorsal root entry zones of C5 and C6 were used for identification of each spinal segment. The dura mater was removed and the spinal cord segments briefly placed in phosphate-buffered saline (PBS) prior to being tested. Transverse slices of 1.99±0.28mm height were dissected out from the spinal cords using a 3-mm biopsy punch resulting in cylindrically shaped portions of white matter collected from the lateral columns. White matter samples were placed on aluminum platens on the test bench system (linear actuator Electroforce3200 equipped with a 10N load cell; TA Instruments, New Castel, DE) and compressed rostro-caudally. The tests were accomplished within one-hour post-mortem. Each test was recorded using a high-frame rate (120 Hz) camera (GoPro Inc., USA) to document the actual sample dimensions (height and diameter) and to monitor any buckling or bulging at maximum compression. Sample diameter and height were used to calculate undeformed area and initial length respectively. Test videos were carefully inspected and samples with any signs of buckling or bulging were removed from further analysis. To reduce inertia effects during loading, the load cell was mounted on the fixed side.

A total of 75 tests were performed; however, despite consistent test conditions and a high precision test system, some samples showed excessive noise (N=4) in the load cell signal that obscured the test data or buckled/bulged during testing (N=6). These 10 samples were removed from further analysis. Samples were compressed for 1mm in four pre-set deformation velocities of

0.5mm/sec, 5.0mm/sec, 50.0mm/sec and 150.0mm/sec where the highest rate was the fastest velocity possible with our test system and other velocities were set so that the resulting strain rates were comparable with previous spinal cord [14] and brain [28,45] white matter studies. The pre-set deformation velocities resulted in groups with strain rates of (mean standard$\pm$ deviation) 0.32$\pm$0.02/sec (ultra-low), 2.83$\pm$0.56/sec (low), 25.47$\pm$4.06/sec (medium) and 77.22$\pm$15.16/sec (high) with 5, 20, 21 and 19 samples respectively. Engineering stress (force over the undeformed area) and strain (machine head displacement over the sample initial height) were calculated for each test. The resulting peak strains varied ($0.19 < \varepsilon < 0.68$) due to variability in the samples' heights and the machine control protocol. To better mimic *in vivo* conditions, samples were not preconditioned in this experiment [14,46]. To ensure a consistent zero position, all the samples were preloaded to 0.05 N before the test started. The stress-relaxation behavior of the NHP white matter was observed by holding the peak strain for 60 seconds and the force and deformation were recorded (sampling time was 0.0004 seconds).

2.2 Statistical analysis

The effect of strain rate on stress was determined using an ANCOVA by comparing stress levels at fixed strain increments (0.1, 0.2, 0.3 and 0.4) between strain rate groups with a Tukey-Kramer post-hoc HSD analysis (α=0.05). Animal weight and age were included as covariates in the model. To evaluate the effect of strain rate on the amount of stress relaxation, the amount of stress relaxed after 60 seconds was normalized against the peak stress for each test, grouped by strain rate, and compared using an ANCOVA with a Tukey-Kramer HSD post-hoc analysis ($\alpha = 0.05$). Again, animal weight and age were included as covariates.

2.3 Constitutive model definition

To find a FE tractable constitutive model that describes the white matter compressive response for large deformation explicit analysis, a hyperelastic material model that best fit the stress-strain response was required. This hyperelastic model was combined with a Prony series expansion to quantify the viscoelastic response of the material [10,14,47,48].

Table 1: Incompressible strain energy functions and the uniaxial engineering stress response for each strain energy function. C_{ij} , μ and α are the material parameters and λ_U is the principal stretch in the uniaxial loading direction. Uniaxial response is obtained from $P_{uniaxial} = \frac{\partial \psi}{\partial \lambda_U} - \frac{1}{\lambda_U} p$, where p is determined using uniaxial loading boundary conditions.

Hyperelastic model	Incompressible energy function	1st Piola-Kirchhoff uniaxial response	Optimization constraints
Mooney-Rivlin	$\psi_1 = C_{10}(I_1 - 3) + C_{01}(I_2 - 3) + p(J-1)$	$P_U^1 = 2(1-\lambda_U^{-3})(C_{10}\lambda_U + C_{01})$	$C_{10} + C_{01} > 0\ ; \frac{C_{10}}{C_{01}} > 1$
Polynomial (N=2)	$\psi_2 = \sum_{i+j=1}^{2} C_{ij}(I_1-3)^i (I_2-3)^j + p(J-1)$	$P_U^2 = 2(1-\lambda_U^{-3})\{C_{10}\lambda_U + C_{01} + 2C_{20}\lambda_U(I_1-3) + C_{02}(I_1 - 3 + \lambda_U(I_2-3)) + 2C_{11}(I_2-3)\}$	$C_{10} + C_{01} > 0$ $\frac{C_{10}}{C_{01}} > 1\ ; \frac{C_{20}}{C_{02}} > 1$
Reduced polynomial (N=2)	$\psi_3 = C_{10}(I_1-3) + C_{20}(I_1-3)^2 + p(J-1)$	$P_U^3 = 2(\lambda_U - \lambda_U^{-2})(C_{10} + 2C_{20}(I_2-3))$	$C_{10} + C_{20} > 0\ ; \frac{C_{10}}{C_{20}} > 1$
Yeoh	$\psi_4 = \sum_{i=1}^{3} C_{i0}(\bar{I}_1 - 3)^i + p(J-1)$	$P_U^4 = 2(\lambda_U - \lambda_U^{-2})(C_{10}\lambda_U + 2C_{20}(I_1-3) + 3C_{30}(I_1-3)^2)$	$C_{10} + C_{30} > 0\ ; \frac{C_{10}}{C_{30}} > 1$
Ogden (1st order)	$\psi_5 = \frac{2\mu}{\alpha^2}(\lambda_1^\alpha + \lambda_2^\alpha + \lambda_3^\alpha - 3)$	$P_U^5 = \frac{2\mu}{\alpha}\left(\lambda_U{}^{\alpha-1} + \lambda_U{}^{-\frac{1}{2}\alpha-1}\right)$	$\alpha > 1\ ;\ \alpha < -1\ ;\ \mu > 0$

Loading data of each strain rate group (i.e. ultralow, low, medium and high) samples were pooled to form a point cloud data for each strain rate group in order to find the average response of the experimental tests. Five well established incompressible isotropic hyperelastic constitutive models (Table 1) were fit to the pooled data. The strain energy function was formulated as,

$$\psi = \psi(I_1, I_2) - p(J-1) \quad or \quad \psi = \psi(\lambda_1, \lambda_2, \lambda_3) - p(J-1) \tag{1}$$

where λ_i ($i = 1,2,3$) are the three principal stretches, I_1 and I_2 are the first and second strain invariants, J is the determinant of the deformation gradient tensor and the p is identified as a hydrostatic pressure [49]. Model parameters were obtained through constrained nonlinear optimization using fmincon (Matlab R2015b, The MathWorks Inc Natick, MA) with a wide range of randomly generated initial guesses to ensure the global minimum was achieved. Drucker stability was imposed in fitting the hyperelastic models while the corresponding constraints (Table 1) were also applied to each model [27,50]. The appropriateness of the model was assessed based on the fit to the data (R^2) and the complexity of the model (i.e. less complex model was preferred).

2.4 Viscoelastic formulation

Quasi-linear viscoelastic (QLV) theory has provided good fits to our prior high strain experimental data for spinal cord white matter [10,14] and has been used in several studies modeling the high strains and strain rates of traumatic spinal cord injury [3,8,10,14]. QLV models have the benefits of being more easily implemented in commercial software and more computationally cost effective in explicit, large deformation, FE models. In addition, the QLV model has been shown to successfully predict the patterns of injury and tissue level stresses/strains in computational studies of SCI [3,8,10]. The QLV model was implemented using the most suitable hyperelastic models identified in the previous section. For the hyperelastic material, the QLV behavior was represented by a Prony series expansion of the dimensionless relaxation modulus applied directly to the strain energy function [27,50],

$$W(t) = \int_0^t \left\{ g_R(t-\tau) \frac{d\psi}{d\tau} \right\} d\tau \qquad (2)$$

where W denotes the time dependent strain energy, t is time, ψ is the hyperelastic strain energy function (Table 1) and $g_R(t)$ is dimensionless relaxation function,

$$g_R(t) = 1 - \sum_{i=1}^{N} g_i(1 - e^{-t/\tau_i}) \quad (3)$$

where $g_i$is the relative moduli and τ_i is the relaxation time of ith term in the Prony series and N is the number of terms in the Prony series.

The optimized parameters were determined through inverse FE analysis by simulating the compressive experiments and fitting the results to the experimental responses (loading portion). The average high and ultralow strain rate group behaviors were each simulated in ABAQUS (v6.14 Dassault Systems Simulia Corp., Providence, RI). The FE models were generated using the average diameter and height of all the samples (h=1.99mm, d=3.59mm) (Figure 1). Models were meshed with 0.15mm continuum elements (C3D8R) following a mesh convergence analysis. The platens were modeled as analytically rigid surfaces. The coefficient of friction (μ) for the contact between the platen and the white matter samples was assumed to be slip rate dependent with μ equal to 0.09, 0.18 and 0.18 at strain rates of 1/sec, 30/sec and 60/sec respectively [51]. ABAQUS linearly interpolates between these values based on the slip rate at the surface to determine the proper coefficient of friction.

Figure 1: (A) White matter sample in the test apparatus, sample is compressed between the two platens. Simulation of the compressive tests in ABAQUS is shown in undeformed (A) and deformed (B) configurations.

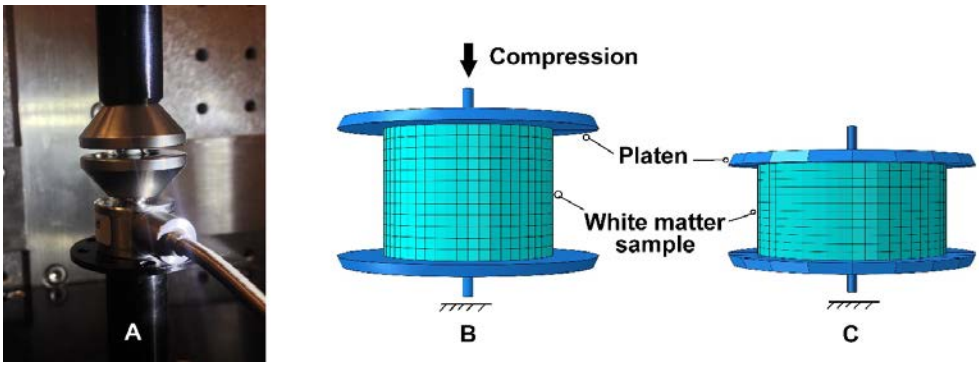

To avoid numerical ill-conditioning caused by a fully incompressible constitutive model definition in the FE implementation, white matter material compressibility was allowed

(υ=0.4995) in the simulations [10,50,52]. The bottom platen was fixed and the samples were compressed by displacing the top platen. The force and displacement of the top platen reference point were recorded to calculate the engineering stresses and strains respectively. In this study, the reduced time constants in the Prony series assumed *a priori* to be approximately equal to the average duration of loading in each strain rate group and our pilot studies showed that a 4-term Prony series was required for this QLV model (i.e. τ_1=0.01sec, τ_2=0.02sec, τ_3=0.2sec and τ_4=2.0sec) [48,53]. A nonlinear constraint optimization algorithm (interior-point, fmincon, MATLAB, R2016b, The MathWorks Inc., Natick, MA), which iteratively invoked a Python code to run the ABAQUS simulations determined the model parameters. The optimization constraints were updated in each iteration based on the previous iteration results. The cyclic procedure continued until the coefficients converged to a single set of coefficients with four decimal accuracy. The corresponding R^2 values were used to quantify the fits.

Once the optimal parameters were determined from optimizing between high and ultralow strain rates, the optimal parameters were implemented to simulate all the four strain rate experiments (loading and relaxation). To assess the fit of each model, the root mean square error (RMSE) of one standard deviation of the experimental data (loading and relaxation) was compared with the RMSE of the fitted model for each strain rate group [54,55]. If the RMSE of the fitted model was less than the RMSE of one standard deviation of the experimental data, the model was considered to be a suitable fit. Furthermore, the model was reviewed to ensure the predicted fit stayed within one standard deviation of the mean experimental data at all time points.

3 RESULTS

3.1 Experimental results

The average peak stresses increased with increased strain rate and peak strain (Figure 2). Strain rate had a significant effect on the stress level in all strain increments ($p < 0.0001$), however, animal age, weight and age-weight interaction did not significantly affect the stress levels. At 10% strain, the high rate data was significantly different from the other rates; however, at the other strain increments (i.e. 20%, 30% and 40%) the high and medium rates were significantly different from low and ultralow but not from each other ($p < 0.05$). For the latter increments, the stress levels at the low and ultralow strain rate groups were also not significantly different from each other (Figure 3). On average, the percent decrease in stress after 60 seconds was significantly ($p < 0.05$) higher in the high (92.7 ± 3.4 %), medium (91.5 ± 5.3 %) and low (88.6 ± 5.3 %) strain rate groups compared to the ultralow group (77.7 ± 2.2 %). Averaged stress-strain responses showed an increase in the stiffness of the material with increased strain rate except for the high strain rate group where the stiffness increased quickly in low strains (<0.1) then decreased (0.1-0.2) and then increased to reach the peak.

Figure 2: NHP spinal cord white matter average compressive stress-strain response grouped by strain rate. Average stress increased by increasing strain rate in all strain rate groups. Error bars show the standard deviation of the stress.

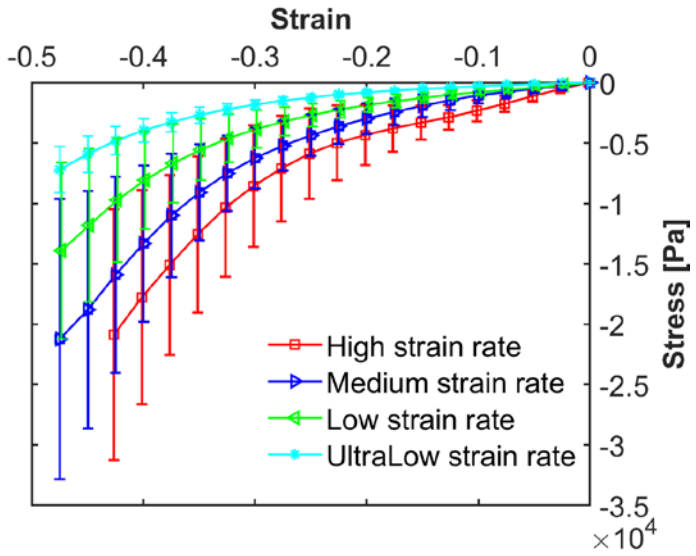

Figure 3: Interquartile ranges (boxes) and medians (lines within each box) of stress levels at 10%, 20%, 30% and 40% strain increments for the four strain rate groups. Whiskers are extended to include the range of all data in the sample group. In each strain rate group, stress levels not connected by the same letter are significantly different (Tukey–Kramer HSD). Labels U, L, M and H refer to ultralow, low, medium and high rate groups respectively

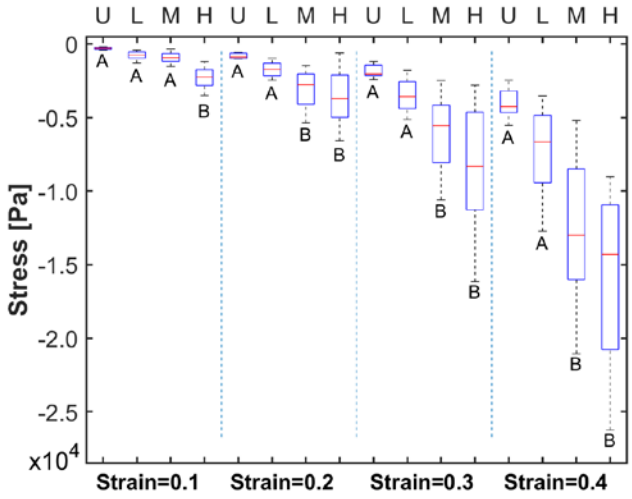

3.2 Constitutive model definition

Experimental variability increased with increasing strain rate across the four groups, with stress coefficients of variations between 0.21-0.28, 0.313-0.52, 0.44-0.75 and 0.49-0.66 for the ultralow,

low, medium and high strain rate groups respectively. The hyperelastic models fit to all experiments at a single strain rate (point cloud data) showed that the 1st order Ogden, Mooney-Rivlin, and Yeoh models better captured the material behavior (Figure 4) in all strain rate groups ($0.82< R^2 <0.86$) compared to the reduced polynomial ($0.58< R^2 <0.74$) and the 2nd order polynomial ($0.14<R^2<0.79$). Although the Yeoh model was able to predict the tissue behavior, this model contains three invariants (compared to Ogden and Mooney-Rivlin with two invariants) which would increase the complexity of the model in the viscoelastic formulation and FE implementation. Therefore, the Mooney-Rivlin and Ogden hyperelastic models were selected to develop the viscoelastic formulation.

Figure 4: Representative pooled stress-strain data points for medium strain rate group. Data for all the samples with same rate group were pooled to form a cloud of data and fit with the hyperelastic models. The fits of the five constitutive models for the medium strain rate compressive response are presented. The average response is also presented in the figure for comparison. Mooney-Rivlin model best fitted the data while polynomial model had the weakest fit in this strain rate group. The Ogden, Mooney-Rivlin and Yeoh model results are coincident for this strain rate group.

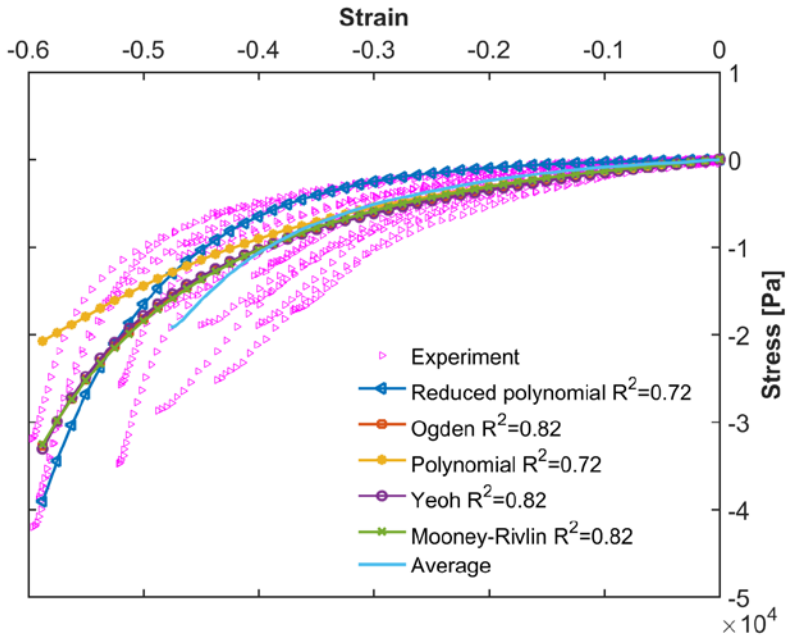

3.3 Results of the viscoelastic fit

RMSEs of one standard deviation from the experimental mean were 2.84kPa, 3.01kPa, 3.33kPa and 5.24kPa for the high, medium, low and ultralow strain rates respectively. Given the variability of the experimental data, the Ogden QLV model (4-term Prony series) with the optimized parameters (Table 2) predicted the material behavior with RMSEs (2.77kPa, 2.60kPa, 2.73kPa and 3.64kPa for high, medium, low and ultralow respectively) that were lower than the experimental RMSEs. The Mooney-Rivlin QLV model (4-term Prony series) also predicted the high, medium and low strain rates with RMSEs of 3.34kPa, 3.02kPa and 3.73kPa respectively, however, was not able to predict the ultralow rate group (RMSE=5.35kPa compared to experiment RMSE=5.24kPa). For both Ogden and Mooney-Rivlin QLV models, the FE responses well fit within the one standard deviation from the mean for high, medium and low strain rate groups (Figure 5-a, b and c).

Table 2: Optimized parameters of 1st order Ogden and Mooney-Rivlin 4-term QLV models. The reduced times for the Prony series were $\tau_1 = 0.01$ sec, $\tau_2 = 0.02$ se c, $\tau_3 = 0.2$ and $\tau_4 = 2.0$ sec.

QLV model	**Model Parameters**					
1st order Ogden	α	μ [kPa]	g_1	g_2	g_3	g_4
	4.63	8.28	0.5296	0.3107	0.0141	0.0016
Mooney-Rivlin	C_{10}[kPa]	C_{01}[kPa]	g_1	g_2	g_3	g_4
	3.27	0.91	0.5256	0.3163	0.1250	0.0071

In the ultralow strain rate regime, the Ogden QLV model loading response fit within the one standard deviation lines, however, the Money-Rivlin QLV loading response was softer than the experiments (Figure 5-d). Increasing the number of Prony series terms beyond four did not affect the accuracy of the predictions in the models.

Figure 5: Ogden and Mooney QLV model predictions for (a) high, (b) medium, (c) low and (d) ultralow strain rate groups. The mean experimental response (blue line) is shown with one standard deviation of the mean (red and yellow lines) to demonstrate the experimental variability. The horizontal axis represents time [sec] in all of the plots. The number of data points have been reduced from original 0.0004 sec for better visualization of the model results.

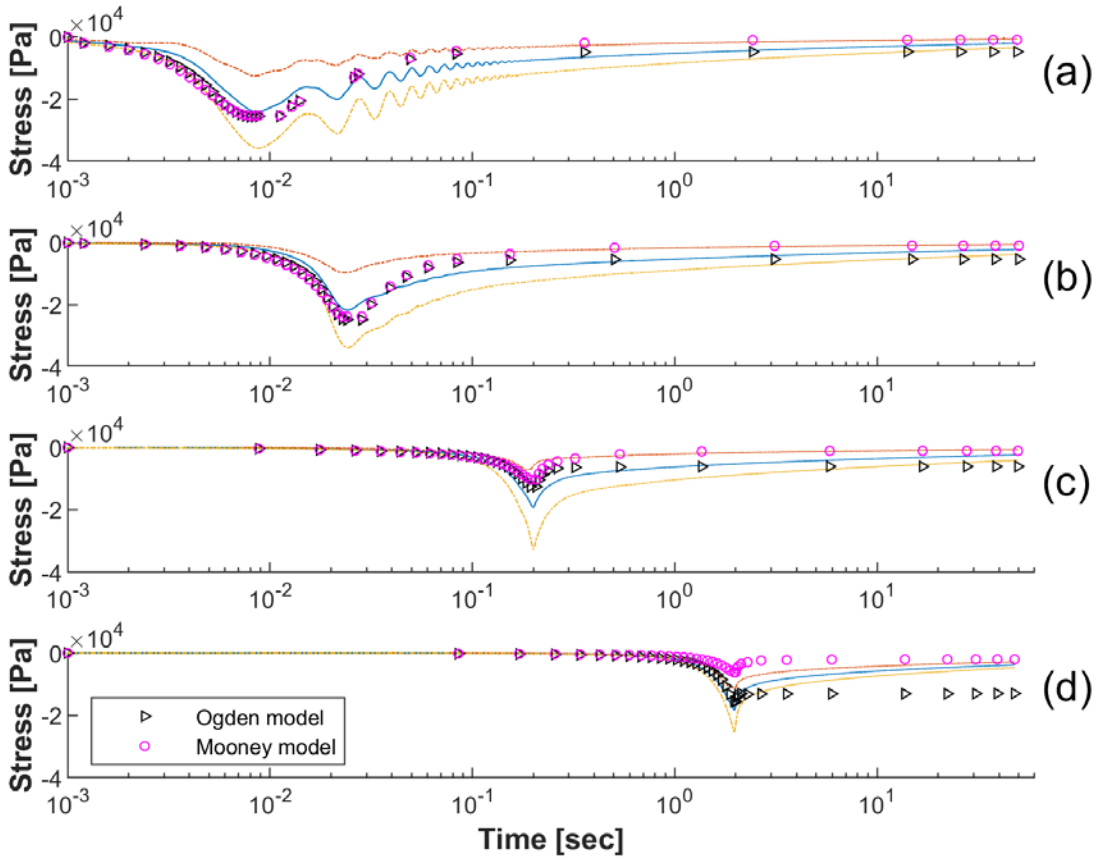

4 DISCUSSION

Variations in the mechanical properties of brain across different species [56–58] suggest that using spinal cord white matter constitutive models obtained from animal tissue tests in human SCI models may introduce inaccuracies. However, testing human tissue is limited by accessibility and post-mortem time effects [42]. Central nervous system tissues in NHPs closely resemble humans [1] and therefore, it is expected that material constitutive models obtained from NHPs will increase the fidelity and the accuracy of human SCI models. As most traumatic SCIs in humans result from

compressive loading on the spinal cord, characterizing the compressive response of the spinal cord white matter to traumatic insults is essential. This study is the first to characterize NHP spinal cord white matter mechanical properties; and is the first to test spinal cord white matter at injurious strain rates ($\dot{\varepsilon}$>10/sec) typical of traumatic SCI, using fresh samples (post-mortem time < 1-hour).

The primary strength of this study was the use of NHP tissues as NHPs more closely resemble humans. Time post-mortem has been shown to have a significant effect on mechanical response of neurological tissues [41,42]. Completing the compressive tests within 1-hour post-mortem should reduce tissue degradation and preserve the tissue integrity. During traumatic SCIs, the spinal cord (and its constituents) experience high strains over a short time; however, due to the lack of experimental data at strain rates typical of traumatic impact, existing viscoelastic models were established using low to moderate strain rate tests and the traumatic injury strain rate response was unclear [10,14,43,54]. The high strain rate tests in this study provide critical information on the viscoelastic behavior of the spinal cord white matter immediately after loading which has manifested itself in the Prony series relaxation times (τ_i's in equation (3)), and have enabled a one order of magnitude reduction in relaxation times (i.e. τ_1=0.01sec compared to 0.1sec<τ_i's in previous studies). This new constitutive model will increase the accuracy of spinal cord FE models in predicting the overall *in vivo* impact mechanics of traumatic impact injuries and the immediate time after injury. Increased model accuracy may provide important insights into the role and timing of decompression on spinal cord stresses.

The NHP spinal cord white matter average compressive response was slightly stiffer than the porcine spinal cord white matter reported at comparable strain rates (low and ultralow) [14]; however, the stiffness difference increased with increasing strain rate (Figure 6). The porcine brain showed a stiffer compressive response at ultralow strain rates [27]; while the bovine brain was

much stiffer than NHP spinal cord white matter in ultralow rates [59]. No higher strain rate data (>5.0/sec) for spinal cord white matter exists for comparison to the medium and high rate groups in this study. NHP white matter showed similar behavior to porcine brain results at medium and high strain rates [28]. However, Rashid and colleagues reported stiffer material properties for porcine brain at comparable strain rates [45] (Figure 6). Considering the experimental variability in both the previous tests and our tests, our results were within the range of reported values of previous studies. The variability in reported experimental results highlight the difficulties in reliably testing this ultra-compliant tissue and the potential confounding effects of numerous experimental variables such as species, structure, location of tissue sampled, postmortem time, processing and storage parameters. The reliability of the data will continue to improve with large scale testing while controlling for or observing and reporting as many of these experimental variables as possible.

The inverse FE modelling method used for optimization in this study has been previously used in brain [26,60–62] parameter characterization. However, previous spinal cord viscoelastic modeling efforts have analytically fit the experimental response to constitutive formulations in order to find the material properties [14,44,54]. As this method does not replicate the material's multiaxial (e.g. transverse) state of loading, it inherently hinders the accuracy of the determined material parameters and the model. The advanced optimization method using inverse FE in this study which directly incorporates FE models of the experimental tests in the parameter optimization, considers the off-axis loading responses, and provides a more accurate FE-adoptable constitutive model for the material.

Figure 6: Comparison of the compressive behavior of spinal cord and brain white matter in different studies based on the applied strain rate. NHP spinal cord white matter was stiffer than porcine white matter in comparable strain rates and was close to brain white matter at higher strain rates. Error bars show standard deviation of the stress.

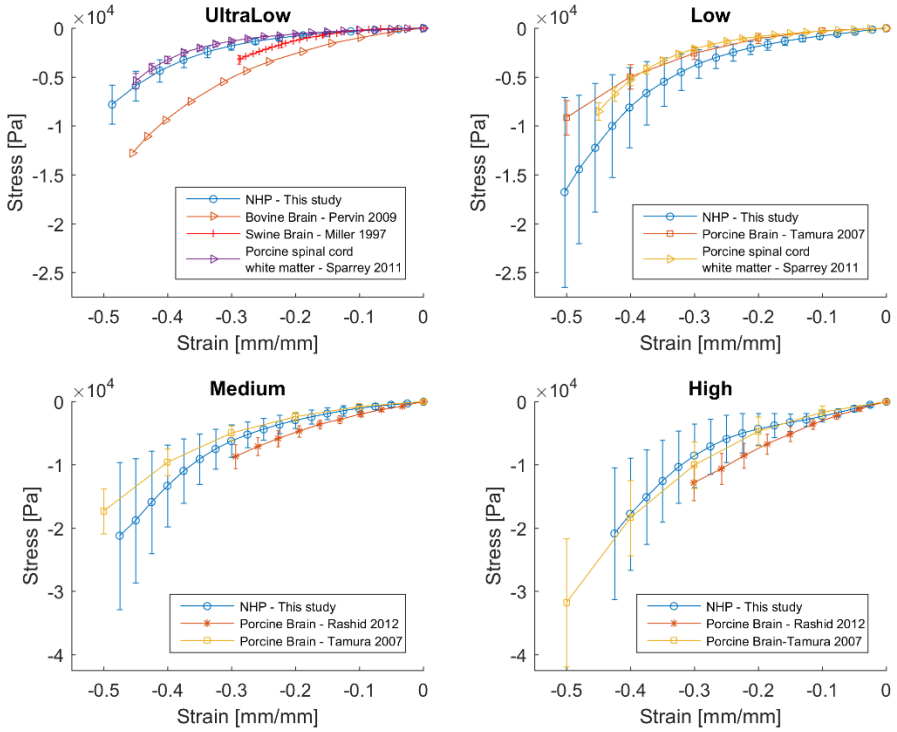

Studies of rat ligaments and the spinal cord suggest that the QLV model is insufficient for predicting these soft tissues' viscoelastic behavior and that fully nonlinear models are required to capture physiological behavior [54,63]. However, these studies investigated the material behavior in low strain ranges (<5%) and did not expand their findings for large strains. For the range of peak strains, at the high strains and strain rates explored in this study, the QLV model was able to capture the material's behavior. A primary strength of the proposed QLV model presented in this study is that the QLV formulation is a built-in model in most commercially available FE software (e.g. ABAQUS) and therefore it is easier to implement in related FE analysis. Further testing of the tissue at a range of peak strains representative of both physiological and injury loading and in both stress relaxation and creep will help to determine if a more complicated material model is

required to represent the tissue response more generally. However, the QLV model was able to simulate the high strain and high strain rate loading typical of traumatic injury.

Efforts in reducing the time post-mortem as well as the complexity of the tissue harvesting process introduced different challenges to this study and caused some limitations. Cutting uniform tissue samples in this ultra-soft tissue at the scale needed for these tests is difficult, however, we tried to reduce human error by using a pre-set 3mm biopsy punch. More importantly, relating machine head displacements to each sample's strain is challenging and may have led to inaccuracies in strain calculations. Our assumption [14,44,47,48] was to consider the machine head displacement as the sample deformation which requires the sample's transverse sections to remain plane in the loading process. The shear contact force generated between the white matter and the platen may have caused violations from the plane sections assumption. In addition, although the camera system (120Hz, GoPro Inc., USA) used in this study was not fast enough to record the entire high strain rate tests, filtering buckled and bulged tests was enabled by combining the recorded frames with the force readouts and visual inspection of the samples at the end of the procedure. The constitutive models presented in this study were limited to characterizing the mechanical response of the tissue to large strains but did not specifically incorporate damage in the material model. Damage may have occurred in the samples compressed beyond their physiological deformation range but structural damage was not directly observed in this study. By not accounting for damage accumulation in this model, the authors acknowledge that this limits the generalizability of the model and may not accurately represent stress softening or subsequent tissue loading – though these are not typically observed in SCI models. Further work will be required to define the structural and functional failure limits for spinal cord white matter and to derive constitutive models capable of incorporating damage. Finally, the filter settings were

changed on the load cell during this series of tests which resulted in a phase lag being introduced in a subset of the data. A correction factor was determined by running similar experiments on surrogate tissue samples to ensure all data was being analyzed on the same timeline [40].

The material constitutive model presented in this study has been characterized based on the compressive behavior of the NHP spinal cord white matter. This material model does not account for the anisotropy of the white matter introduced by the presence of axonal fibers [10,18]. Therefore, the accuracy of the presented constitute model is limited to compressive loading cases. Extrapolating these results to capture the material's tensile behavior or to model the multi-axial loading state of the spinal cord during SCI without including anisotropy may hinder the ability of the SCI model to correlate tissue damage to the mechanical outcomes [10]. Further tensile/shear experimental tests are required to determine the anisotropic behavior of NHP white matter and integrate those results to improve the capability of the current constitutive model. However, due to the scale of the NHP spinal cord white matter samples, conducting tensile and shear tests will be highly complex [64].

Directly measuring spinal cord white matter tissue properties in the body would be ideal; however, current technologies are insufficient for isolating white matter tissue properties at the high speeds and high strains typical of injury. While non-invasive magnetic resonance elastography (MRE) methods may have the potential to characterize spinal cord tissue in-vivo; the feasibility of MRE for characterizing spinal cord tissue has not been validated [65]. Although MRE has been used to characterize brain tissue and differentiate in-vivo versus in vitro responses of brain tissues assuming isotropy [66–72] or transverse isotropy [73], current MRE applications are limited to strains that are insufficient for characterizing the large strains associated with the highly

nonlinear SCI phenomenon. In addition, isolating spinal cord white matter might be challenging in MRE methods due to the small sizes of the tissue compared to MRE wavelengths [74].

Using NHPs to study SCI has been widely revisited recently [1,75,76] since these models increase the fidelity and reliability of SCI models in transferring pre-clinical findings to humans [75]. However, primates are highly variable morphologically (i.e. weight, skeleton, etc.) and much more expensive than other animal models (e.g. rodents, porcine, etc.). FE models are a critical step in generating a predictable injury foundation as well as improving the repeatability of the models by providing insight to SCI mechanisms and injury mechanics. Similarly, human FE models of SCI are critical for assessing mechanical injury prevention strategies (e.g. helmets, seatbelts, etc.) and may provide insight into the mechanisms of clinical treatments (e.g. decompression surgery). Susceptibility of FE model outcomes (such as patterns of injury) to predefined material constitutive models [8,10,77] highlights the need for accurate characteristics for the constituent materials. So far, computational human SCI models have extrapolated their material properties from rodents, pigs and bovine [4,11]. Our study provides NHP spinal cord material characteristics that eliminate the need for extrapolating these material properties from heterogeneous animals.

5 CONCLUSION

In conclusion, we showed that NHP spinal cord white matter is highly sensitive to loading rate, specifically, it is substantially stiffer at very high loading rates typical of traumatic SCI. In this study we determined the constitutive properties of the isotropic spinal cord white matter glial matrix. Further experiments will be required to quantify the contributions of the embedded axonal fibers to NHP white matter anisotropy. The constitutive model evaluation demonstrated that at large deformations both loading and relaxation regimes of the NHP spinal cord compressive

behavior are adequately captured by a QLV model. Importantly, our results showed the NHP spinal cord white matter to have similar properties to those previously reported for porcine spinal cord white matter and brain white matter in compression. This indicates that constitutive models derived from these other tissue sources may provide an adequate representation of spinal cord white matter characteristics without requiring the logistical and ethical complexities of accessing fresh NHP or human tissues.

Acknowledgements

This work was supported by grants from the Natural Sciences and Engineering Research Council of Canada (EQPE-Q407572, RGPIN-402007), the VA, UCSF Department of Neurosurgery and the CH Neilsen Foundation.

6 REFERENCES

[1] E.A. Salegio, J.C. Bresnahan, C.J. Sparrey, W. Camisa, J. Fischer, J. Leasure, J. Buckley, Y.S. Nout-Lomas, E.S. Rosenzweig, R. Moseanko, S. Strand, S. Hawbecker, M.-J. Lemoy, J. Haefeli, X. Ma, J.L. Nielson, V.R. Edgerton, A.R. Ferguson, M.H. Tuszynski, M.S. Beattie, A Unilateral Cervical Spinal Cord Contusion Injury Model in Non-Human Primates (Macaca mulatta)., J. Neurotrauma. 33 (2016) 439–59. doi:10.1089/neu.2015.3956.

[2] C.H. Tator, Review Of Treatment Trials In Humanspinal Cord Injury: Issues, Difficulties, And Recommendations, Neurosurgery. 59 (2006) 957–987. doi:10.1227/01.NEU.0000245591.16087.89.

[3] C.M. Russell, A.M. Choo, W. Tetzlaff, T. Chung, T.R. Oxland, Maximum principal strain correlates with spinal cord tissue damage in contusion and dislocation injuries in the rat cervical spine, J. Neurotrauma. 29 (2012) 1574–1585.

[4] C.Y. Greaves, M.S. Gadala, T.R. Oxland, A three-dimensional finite element model of the cervical spine with spinal cord: An investigation of three injury mechanisms, Ann. Biomed. Eng. 36 (2008) 396–405. doi:10.1007/s10439-008-9440-0.

[5] B. Galle, H. Ouyang, R. Shi, E. Nauman, Correlations between tissue-level stresses and strains and cellular damage within the guinea pig spinal cord white matter, J. Biomech. 40 (2007) 3029–3033. doi:10.1016/j.jbiomech.2007.03.014.

[6] L. Bilston, Finite element analysis of some cervical spinal cord injury modes, IRCOBI Conf. Biomech. …. (1998). https://trid.trb.org/view.aspx?id=685098 (accessed May 1, 2017).

[7] C.J. Sparrey, G.T. Manley, T.M. Keaveny, Effects of white, grey, and pia mater properties on tissue level stresses and strains in the compressed spinal cord., J. Neurotrauma. 26 (2009)

585–595.

[8] J.T. Maikos, Z. Qian, D. Metaxas, D.I. Shreiber, Finite element analysis of spinal cord injury in the rat, J. Neurotrauma. 25 (2008) 795–816.

[9] Y. Imajo, I. Hiiragi, Y. Kato, T. Taguchi, Use of the finite element method to study the mechanism of spinal cord injury without radiological abnormality in the cervical spine., Spine (Phila. Pa. 1976). 34 (2009) E83-7. doi:10.1097/BRS.0b013e31818a2c30.

[10] S. Jannesar, B. Nadler, C.J. Sparrey, The Transverse Isotropy of Spinal Cord White Matter Under Dynamic Load, J. Biomech. Eng. 138 (2016) 91004. doi:10.1115/1.4034171.

[11] H. Kimpara, Y. Nakahira, M. Iwamoto, K. Miki, K. Ichihara, S. Kawano, T. Taguchi, Investigation of anteroposterior head-neck responses during severe frontal impacts using a brain-spinal cord complex FE, Stapp Car Crash J. 50 (2006) 509–544.

[12] A.M. Choo, J. Liu, C.K. Lam, M. Dvorak, W. Tetzlaff, T.R. Oxland, Contusion, dislocation, and distraction: primary hemorrhage and membrane permeability in distinct mechanisms of spinal cord injury, J. Neurosurg. Spine. 6 (2007) 255–266.

[13] G.A. Metz, A. Curt, H. van de Meent, I. Klusman, M.E. Schwab, V. Dietz, Validation of the weight-drop contusion model in rats: a comparative study of human spinal cord injury., J. Neurotrauma. 17 (2000) 1–17. http://www.ncbi.nlm.nih.gov/pubmed/10674754 (accessed September 11, 2015).

[14] C.J. Sparrey, T.M. Keaveny, Compression behavior of porcine spinal cord white matter, J. Biomech. 44 (2011) 1078–1082. doi:10.1016/j.jbiomech.2011.01.035.

[15] J.C. Gensel, C.A. Tovar, F.P.T. Hamers, R.J. Deibert, M.S. Beattie, J.C. Bresnahan, Behavioral and Histological Characterization of Unilateral Cervical Spinal Cord Contusion

Injury in Rats, J. Neurotrauma. 23 (2006) 36–54. doi:10.1089/neu.2006.23.36.

[16] T. Bhatnagar, J. Liu, A. Yung, P.A. Cripton, P. Kozlowski, T. Oxland, In Vivo Measurement of Cervical Spinal Cord Deformation During Traumatic Spinal Cord Injury in a Rodent Model., Ann. Biomed. Eng. (2015). doi:10.1007/s10439-015-1412-6.

[17] J. Lee, F. Streijger, S. Tigchelaar, M. Maloon, A contusive model of unilateral cervical spinal cord injury using the infinite horizon impactor, JoVE. (2012). https://www.jove.com/video/3313/a-contusive-model-unilateral-cervical-spinal-cord-injury-using (accessed February 25, 2017).

[18] B. Galle, H. Ouyang, R. Shi, E. Nauman, A transversely isotropic constitutive model of excised guinea pig spinal cord white matter, J. Biomech. 43 (2010) 2839–2843. doi:10.1016/j.jbiomech.2010.06.014.

[19] H. Ouyang, B. Galle, J. Li, E. Nauman, R. Shi, Biomechanics of spinal cord injury: a multimodal investigation using ex vivo guinea pig spinal cord white matter., J. Neurotrauma. 25 (2008) 19–29. doi:10.1089/neu.2007.0340.

[20] G.B. Shellswell, D.J. Restall, V.C. Duance, A.J. Bailey, IDENTIFICATION AND DIFFERENTIAL DISTRIBUTION OF COLLAGEN TYPES IN THE, North-Holl. Biomed. Press. 106 (1979) 305–308.

[21] A.J.M. Spencer, Continuum theory of the mechanics of fibre-reinforced composites, Springer, New York, 1984. http://link.springer.com/content/pdf/10.1007/978-3-7091-4336-0.pdf (accessed October 9, 2014).

[22] A.E. Green, Large elastic deformations, Oxford, UK, 1971. http://onlinelibrary.wiley.com/doi/10.1111/j.1475-1305.1971.tb01733.x/full (accessed

November 14, 2016).

[23] G.A. Holzapfel, T.C. Gasser, R.A.Y.W. Ogden, A New Constitutive Framework for Arterial Wall Mechanics and a Comparative Study of Material Models, J. Elast. Phys. Sci. Solids. 61 (2000) 1–48.

[24] J. a. Weiss, B.N. Maker, S. Govindjee, Finite element implementation of incompressible, transversely isotropic hyperelasticity, Comput. Methods Appl. Mech. Eng. 135 (1996) 107–128.

[25] S. Chatelin, C. Deck, R. Willinger, An anisotropic viscous hyperelastic constitutive law for brain material finite-element modeling, J. Biorheol. 27 (2012) 26–37. doi:10.1007/s12573-012-0055-6.

[26] X. Ning, Q. Zhu, Y. Lanir, S.S. Margulies, A transversely isotropic viscoelastic constitutive equation for brainstem undergoing finite deformation., J. Biomech. Eng. 128 (2006) 925–933. doi:10.1115/1.2354208.

[27] K. Miller, K. Chinzei, Constitutive modelling of brain tissue: experiment and theory., J. Biomech. 30 (1997) 1115–1121.

[28] A. Tamura, S. Hayashi, I. Watanabe, K. Nagayama, T. Matsumoto, Mechanical Characterization of Brain Tissue in High-Rate Compression, J. Biomech. Sci. Eng. 2 (2007) 115–126. doi:10.1299/jbse.2.115.

[29] S. Cheng, L.E. Bilston, Unconfined compression of white matter, J. Biomech. 40 (2007) 117–124. doi:10.1016/j.jbiomech.2005.11.004.

[30] M. Hrapko, J. a W. Van Dommelen, G.W.M. Peters, J.S.H.M. Wismans, Characterisation of the mechanical behaviour of brain tissue in compression and shear, Biorheology. 45

(2008) 663–676. doi:10.3233/BIR-2008-0512.

[31] M. Estes, M.J.- Mechanical, undefined 1970, Response of brain tissue to compressive loading, … -Amer Soc Mech. Eng 345 E …. (n.d.).

[32] F. Pervin, W.W. Chen, Effect of inter-species, gender, and breeding on the mechanical behavior of brain tissue., Neuroimage. 54 Suppl 1 (2011) S98-102. doi:10.1016/j.neuroimage.2010.03.077.

[33] L. Schnell, S. Fearn, H. Klassen, M.E. Schwab, V.H. Perry, Acute inflammatory responses to mechanical lesions in the CNS: differences between brain and spinal cord, Eur. J. Neurosci. 11 (1999) 3648–3658. doi:10.1046/j.1460-9568.1999.00792.x.

[34] P.E. Batchelor, S. Tan, T.E. Wills, M.J. Porritt, D.W. Howells, Comparison of Inflammation in the Brain and Spinal Cord following Mechanical Injury, J. Neurotrauma. 25 (2008) 1217–1225. doi:10.1089/neu.2007.0308.

[35] K. Ichihara, T. Taguchi, I. Sakuramoto, S. Kawano, S. Kawai, Mechanism of the spinal cord injury and the cervical spondylotic myelopathy: new approach based on the mechanical features of the spinal cord white and gray matter., J. Neurosurg. 99 (2003).

[36] S.S. Shetye, M.M. Deault, C.M. Puttlitz, Biaxial response of ovine spinal cord dura mater, J. Mech. Behav. Biomed. Mater. 34 (2014) 146–153. doi:10.1016/j.jmbbm.2014.02.014.

[37] M.M. Panjabi, M. Kifune, L. Wen, M. Arand, T.R. Oxland, R.-M. Lin, W.-S.S. Yoon, A. Vasavada, Dynamic Canal Encroachment During Thoracolumbar Burst Fractu... : Clinical Spine Surgery, J. Spinal Disord. 8 (1995) 39–48.

[38] R.K. Wilcox, T.O. Boerger, R.M. Hall, D.C. Barton, D. Limb, R.A. Dickson, Measurement of canal occlusion during the thoracolumbar burst fracture process, J. Biomech. 35 (2002)

381–384. doi:10.1016/S0021-9290(01)00180-4.

[39] C.J. Sparrey, The effect of impact velocity on acute spinal cord injury, University of British Columbia, 2004. doi:10.14288/1.0080718.

[40] C.J. Sparrey, E.A. Salegio, W. Camisa, H. Tam, M.S. Beattie, J.C. Bresnahan, Mechanical Design and Analysis of a Unilateral Cervical Spinal Cord Contusion Injury Model in Non-Human Primates., J. Neurotrauma. (2016). doi:10.1089/neu.2015.3974.

[41] A. Garo, M. Hrapko, J.A.W. van Dommelen, G.W.M. Peters, Towards a reliable characterisation of the mechanical behaviour of brain tissue: The effects of post-mortem time and sample preparation, Biorheology. 44 (2007) 51–58.

[42] R.J. Oakland, R.M. Hall, R.K. Wilcox, D.C. Barton, The biomechanical response of spinal cord tissue to uniaxial loading., Proc. Inst. Mech. Eng. H. 220 (2006) 489–492. doi:10.1243/09544119JEIM135.

[43] L.E. Bilston, L.E. Thibault, The mechanical properties of the human cervical spinal cord in vitro, Ann. Biomed. Eng. 24 (1996) 67–74.

[44] K. Ichihara, T. Taguchi, Y. Shimada, I. Sakuramoto, S. Kawano, S. Kawai, Gray matter of the Bovine cervical spinal cord is mechanically more rigid and fragile than the white matter, J. Neurotrauma. 18 (2001) 361–367.

[45] B. Rashid, M. Destrade, M.D. Gilchrist, Mechanical characterization of brain tissue in compression at dynamic strain rates., J. Mech. Behav. Biomed. Mater. 10 (2012) 23–38. doi:10.1016/j.jmbbm.2012.01.022.

[46] A. Gefen, S.S. Margulies, Are in vivo and in situ brain tissues mechanically similar?, J. Biomech. 37 (2004) 1339–1352. doi:10.1016/j.jbiomech.2003.12.032.

[47] K. Miller, Method of testing very soft biological tissues in compression, J. Biomech. 38 (2005) 153–158. doi:10.1016/j.jbiomech.2004.03.004.

[48] K. Miller, How to test very soft biological tissues in extension?, J. Biomech. 34 (2001) 651–657. doi:10.1016/S0021-9290(00)00236-0.

[49] G. Holzapfel, Nonlinear Solid Mechanics: A Continuum Approach for Engineering, (2000). http://www.citeulike.org/group/2006/article/1044720 (accessed January 27, 2017).

[50] Abaqus 6.14 Documentation, (2016). http://abaqus.software.polimi.it/texis/search/?query=nearly+incompressible&submit.x=0&submit.y=0&group=bk&CDB=v6.14 (accessed April 5, 2017).

[51] B. Rashid, M. Destrade, M.D. Gilchrist, Determination of friction coefficient in unconfined compression of brain tissue, J. Mech. Behav. Biomed. Mater. 14 (2012) 163–171. doi:10.1016/j.jmbbm.2012.05.001.

[52] J.T. Maikos, R.A.I. Elias, D.I. Shreiber, Mechanical properties of dura mater from the rat brain and spinal cord., J. Neurotrauma. 25 (2008) 38–51. doi:10.1089/neu.2007.0348.

[53] K. Miller, Constitutive model of brain tissue suitable for finite element analysis of surgical procedures., J. Biomech. 32 (1999) 531–537. doi:10.1016/S0021-9290(99)00010-X.

[54] S.S. Shetye, K.L. Troyer, F. Streijger, J.H.T. Lee, B.K. Kwon, P. a. Cripton, C.M. Puttlitz, Nonlinear viscoelastic characterization of the porcine spinal cord, Acta Biomater. 10 (2014) 792–797. doi:10.1016/j.actbio.2013.10.038.

[55] K.L. Troyer, C.M. Puttlitz, Human cervical spine ligaments exhibit fully nonlinear viscoelastic behavior, Acta Biomater. 7 (2011) 700–709. doi:10.1016/j.actbio.2010.09.003.

[56] J. Galford, J. McElhaney, A viscoelastic study of scalp, brain, and dura, J. Biomech. (1970). http://www.sciencedirect.com/science/article/pii/0021929070900072 (accessed April 26, 2017).

[57] M. Prange, D. Meaney, S. Margulies, Defining brain mechanical properties: effects of region, direction, and species., Stapp Car Crash J. (2000). http://europepmc.org/abstract/med/17458728 (accessed April 26, 2017).

[58] S. Chatelin, A. Constantinesco, R. Willinger, Fifty years of brain tissue mechanical testing: From in vitro to in vivo investigations, Biorheology. 47 (2010) 255–276. doi:10.3233/BIR-2010-0576.

[59] F. Pervin, W.W. Chen, Dynamic mechanical response of bovine gray matter and white matter brain tissues under compression., J. Biomech. 42 (2009) 731–5. doi:10.1016/j.jbiomech.2009.01.023.

[60] M.S. Chafi, V. Dirisala, G. Karami, M. Ziejewski, A finite element method parametric study of the dynamic response of the human brain with different cerebrospinal fluid constitutive properties., Proc. Inst. Mech. Eng. H. 223 (2009) 1003–1019. doi:10.1243/09544119JEIM631.

[61] Y. Feng, R.J. Okamoto, R. Namani, G.M. Genin, P. V. Bayly, Measurments of mechanical anisotropy in brain tissue and implications for transversely isotropic material models of white matter, J. Mech Behav Biomed Maetr. 23 (2013) 117–132. doi:10.1016/j.jmbbm.2013.04.007.Measurements.

[62] R. Moran, J.H. Smith, J.J. García, Fitted hyperelastic parameters for Human brain tissue from reported tension, compression, and shear tests, J. Biomech. 47 (2014) 3762–3766.

doi:10.1016/j.jbiomech.2014.09.030.

[63] P. Provenzano, R. Lakes, T. Keenan, Nonlinear ligament viscoelasticity, Ann. Biomed. Eng. (2001). https://link.springer.com/article/10.1114/1.1408926 (accessed September 13, 2017).

[64] S. Budday, G. Sommer, J. Haybaeck, P. Steinmann, G.A. Holzapfel, E. Kuhl, Rheological characterization of human brain tissue, Acta Biomater. 60 (2017) 315–329. doi:10.1016/j.actbio.2017.06.024.

[65] S.A. Kruse, A. Kolipaka, A. Manduca, R.L. Ehman, Feasibility of Evaluating the Spinal Cord with MR Elastography, in: Intl. Soc. Mag. Reson. Med. , 2009: p. 630. https://pdfs.semanticscholar.org/ce41/b90e4945248357ba956e80ad36ba103c249f.pdf.

[66] S.M. Atay, C.D. Kroenke, A. Sabet, P. V. Bayly, Measurement of the Dynamic Shear Modulus of Mouse Brain Tissue In Vivo by Magnetic Resonance Elastography, J. Biomech. Eng. 130 (2008) 21013. doi:10.1115/1.2899575.

[67] Y. Feng, E.H. Clayton, Y. Chang, R.J. Okamoto, P. V Bayly, Viscoelastic properties of the ferret brain measured in vivo at multiple frequencies by magnetic resonance elastography., J. Biomech. 46 (2013) 863–70. doi:10.1016/j.jbiomech.2012.12.024.

[68] M.A. Green, L.E. Bilston, R. Sinkus, In vivo brain viscoelastic properties measured by magnetic resonance elastography, NMR Biomed. 21 (2008) 755–764. doi:10.1002/nbm.1254.

[69] J. Craven, Spinal cord, Anaesth. Intensive Care Med. 5 (2004) 144–146. http://www.sciencedirect.com/science/article/pii/S1472029906003158.

[70] C.L. Johnson, M.D.J. McGarry, E.E.W. Van Houten, J.B. Weaver, K.D. Paulsen, B.P.

Sutton, J.G. Georgiadis, Magnetic resonance elastography of the brain using multishot spiral readouts with self-navigated motion correction, Magn. Reson. Med. 70 (2013) 404–412. doi:10.1002/mrm.24473.

[71] D. Klatt, U. Hamhaber, P. Asbach, J. Braun, I. Sack, Noninvasive assessment of the rheological behavior of human organs using multifrequency MR elastography: a study of brain and liver viscoelasticity, Phys. Med. Biol. 52 (2007) 7281–7294. doi:10.1088/0031-9155/52/24/006.

[72] C.A. Guertler, R.J. Okamoto, J.L. Schmidt, A.A. Badachhape, C.L. Johnson, P. V Bayly, Mechanical properties of porcine brain tissue in vivo and ex vivo estimated by MR elastography., J. Biomech. 69 (2018) 10–18. doi:10.1016/j.jbiomech.2018.01.016.

[73] S.A. Geissler, C.E. Schmidt, T. Schallert, Rodent Models and Behavioral Outcomes of Cervical Spinal Cord Injury., J. Spine. Suppl 4 (2013). doi:10.4172/2165-7939.S4-001.

[74] S.M. Atay, C.D. Kroenke, A. Sabet, P. V. Bayly, Measurement of the Dynamic Shear Modulus of Mouse Brain Tissue In Vivo by Magnetic Resonance Elastography, J. Biomech. Eng. 130 (2008) 21013. doi:10.1115/1.2899575.

[75] B.K. Kwon, A. Ghag, L. Reichl, M.F. Dvorak, J. Illes, W. Tetzlaff, Opinions on the preclinical evaluation of novel therapies for spinal cord injury: a comparison between researchers and spinal cord-injured individuals., J. Neurotrauma. 29 (2012) 2367–74. doi:10.1089/neu.2012.2479.

[76] G. Courtine, M.B. Bunge, J.W. Fawcett, R.G. Grossman, J.H. Kaas, R. Lemon, I. Maier, J. Martin, R.J. Nudo, A. Ramon-Cueto, E.M. Rouiller, L. Schnell, T. Wannier, M.E. Schwab, V.R. Edgerton, Can experiments in nonhuman primates expedite the translation of

treatments for spinal cord injury in humans?, Nat. Med. 13 (2007) 561–6. doi:10.1038/nm1595.

[77] C.J. Sparrey, A.M. Choo, J. Liu, W. Tetzlaff, T.R. Oxland, The Distribution of Tissue Damage in the Spinal Cord Is Influenced by the Contusion Velocity, Spine (Phila. Pa. 1976). 33 (2008) E812–E819. doi:10.1097/BRS.0b013e3181894fd3.